# Oligomerization of Epidermal Growth Factor Receptors on A431 Cells Studied by Time-resolved Fluorescence Imaging Microscopy. A Stereochemical Model for Tyrosine Kinase Receptor Activation

**Theodorus W. J. Gadella, Jr. and Thomas M. Jovin**

Department of Molecular Biology, Max Planck Institute for Biophysical Chemistry, D-37018 Goettingen, Federal Republic of Germany

*Abstract.* The aggregation states of the epidermal growth factor receptor (EGFR) on single A431 human epidermoid carcinoma cells were assessed with two new techniques for determining fluorescence resonance energy transfer: donor photobleaching fluorescence resonance energy transfer (pbFRET) microscopy and fluorescence lifetime imaging microscopy (FLIM). Fluorescein-(donor) and rhodamine-(acceptor) labeled EGF were bound to the cells and the extent of oligomerization was monitored by the spatially resolved FRET efficiency as a function of the donor/acceptor ratio and treatment conditions. An average FRET efficiency of 5% was determined after a low temperature (4°C) incubation with the fluorescent EGF analogs for 40 min. A subsequent elevation of the temperature for 5 min caused a substantial increase of the average FRET efficiency to 14% at 20°C and 31% at 37°C. In the context of a two-state (monomer/dimer) model for the EGFR, these FRET efficiencies were consistent with minimal average receptor dimerizations of 13, 36, and 69% at 4, 20, and 37°C, respectively. A431 cells were pretreated with the monoclonal antibody mAb 2E9 that specifically blocks EGF binding to the predominant population of low affinity EGFR (15). The average FRET efficiency increased dramatically to 28% at 4°C, indicative of a minimal receptor dimerization of 65% for the subpopulation of high affinity receptors. These results are in accordance with prior studies indicating that binding of EGF leads to a fast and temperature-dependent microclustering of EGFR, but suggest in addition that the high affinity functional subclass of receptors on quiescent A431 cells are present in a predimerized or oligomerized state. We propose that the transmission of the external ligand-binding signal to the cytoplasmic domain is effected by a concerted relative rotational rearrangement of the monomeric units comprising the dimeric receptor, thereby potentiating a mutual activation of the tyrosine kinase domains.

EPIDERMAL growth factor (EGF)[1] is a mitogen of 53 amino acids that stimulates the proliferation and differentiation of numerous cell types, particularly of epithelial lineage (for reviews see 6, 7, 50). The EGF receptor (EGFR) is a single polypeptide chain (1186 amino acids) of 170 kD that spans the membrane once via an α-helical segment of 23 hydrophobic amino acids. The extracellular domain (621 amino acids) is heavily glycosylated (contributing 40 kD to the molecular mass) and contains the EGF-binding site. The intracellular domain (542 amino acids) is the locus of a latent tyrosine kinase, the ligand-dependent activation of which leads to autophosphorylation and phosphorylation of exogenous substrates. The growth factor tyrosine kinase receptor (TKR) activates many proteins directly or indirectly, thereby modulating their effector function in signal transduction (for reviews see references 5, 43, 50). Some examples are phospholipase C-γ1 (PLC-γ1), phosphatidylinositol-3′-kinase (PI3-kinase), and the ras GTPase–activating protein (ras GAP). These signal transduction proteins interact physically with the autophosphorylated receptor via SH2 domains (second domain of src homology) conferring high specificity and affinity (44), and leading to the formation of multicomponent signal transduction complexes. A linkage has been recently demonstrated between the activation of EGFR and that of the oncogenic GTP-binding protein Ras (for review see reference 41), mediated via two

Address all correspondence to Dr. T. M. Jovin, Department of Molecular Biology, Max Planck Institute for Biophysical Chemistry, Postfach 2841, D-37018 Goettingen, FRG. Tel.: 49 551 2011381. Fax: 49 551 2011467.

The current address of T. W. J. Gadella, Jr. is Department of Biochemistry, Agricultural University of Wageningen, NL-6703 HA Wageningen, The Netherlands.

1. *Abbreviations used in this paper*: EGF, epidermal growth factor; EGFR, EGF receptor; FRET, fluorescence resonance energy transfer; Fl-EGF, fluorescein-EGF; FLIM, fluorescence lifetime imaging microscopy; MCP, microchannel-plate; pbFRET, FRET based on donor-photobleaching; Rh-EGF, tetramethyl-rhodamine-EGF; TKR, tyrosine kinase receptor.

intermediary proteins, Grb2 (growth factor receptor–binding protein) and guanine nucleotide-releasing factor Sos. Grb2 bridges activated TKR and Sos, leading to a translocation of the latter to the plasma membrane where it induces the exchange of GDP for GTP on Ras. GTP-Ras binds to RAF-1–kinase, thereby initiating the MAP-kinase cascade resulting in the direct phosphorylation of transcription factors and ultimately eliciting the primary mitogenic response, stimulation of DNA replication, and cell division (34, 36).

The regulation by EGF of cellular proliferation constitutes the first signal transduction pathway that can be traced from the plasma membrane to the nucleus without obvious gaps in the mechanism. However, the initial steps in EGFR activation (for reviews see references 40, 43, 50) remain controversial. Two models have been proposed. The first stipulates that external binding of the growth hormone stimulates the tyrosine kinase activity in the cytoplasmic domain via an unspecified conformational change transmitted through the single membrane-spanning region. Two observations support this hypothesis. A single mutation of one amino acid in the membrane-spanning segment of the receptor yields a constitutively activated receptor (tyrosine kinase) uncoupled to EGF binding (48). Secondly, immobilization of purified receptor on affinity columns or dilution in detergent solution also lead to activation of the tyrosine kinase (6). The alternative more generally accepted model, denoted allosteric receptor oligomerization (56, 57) (for reviews see references 40, 50), invokes an intermolecular mechanism in which EGF binding promotes receptor dimerization, the consequences of which are enhanced affinity for the growth factor and activation of the TKR. Evidence for this model derives from several independent observations: electron microscopy of immunogold-labeled receptors shows gold particle clustering upon administration of EGF (51); divalent antibodies directly activate the receptor in the absence of EGF (46); the activation kinetics using solubilized receptors have a second order dependence on receptor concentration (57); and chemical cross-linking studies confirm the occurrence of EGF-induced (13, 18) or covalently stabilized (45) receptor dimerization.

Most of the studies of the EGFR have been performed on A431 cells or membranes derived thereof. A431 is an established human epidermoid cancer cell line overexpressing cell surface EGFR to a level of up to $2 \times 10^6$ receptors/cell and secreting large quantities of the extracellular domain (16, 49). In this and other cell lines (59) two populations of receptors are present with different affinities for EGF: low affinity EGFR ($K_d > 1$ nM) and high affinity EGFR ($K_d < 1$ nM). In A431 cells, the high affinity receptors comprise ~2–12% of the total (14, 19, 37, 59). Defize and colleagues have described a monoclonal antibody, mAb 2E9, that specifically blocks EGF binding to the low affinity sites (15). EGF-dependent signal transduction is retained in cells exposed to mAb-2E9, suggesting that the high affinity–receptor population (2–12%) is necessary and sufficient for EGF function (15). The combined observations that dimerization of the EGFR parallels receptor (tyrosine kinase) activation (3, 46, 56, 57), that receptor dimerization increases the affinity for EGF (3, 56, 57), and that signal transduction can be effected via the high affinity receptors alone (2, 15, 57) clearly demonstrate a correlation between binding to the high affinity EGFR, receptor dimerization, and receptor activation. It has been proposed that the high affinity receptor is associated preferentially with the cytoskeleton (37, 52, 53, 59), suggesting an essential role of the cytoskeleton in the transmission of the signal (24).

Despite the mass of experimental evidence, the inference that ligand-induced dimerization is a prerequisite for tyrosine kinase activation has been questioned repeatedly (10), particularly in view of the fact that most studies performed with the overexpressing A431 cells have dealt with the total EGFR population, most members of which are of the nonfunctional low affinity class. In addition, many of the investigations have dealt with EGFR in membrane fragments, in detergent-stabilized extracts, or reconstituted into lipid bilayers. None of these conditions can be presumed to mimic the native cellular environment in its entirety.

We have studied the phenomenon of receptor oligomerization using newly developed techniques based on the quantitative determination of fluorescence resonance energy transfer (FRET) in the microscope, i.e., with retention of spatial resolution. The basis of FRET is the transfer of excited state energy from a donor fluorescent group to an appropriate light absorbing acceptor molecule. This process takes place only over very short distances (generally <10 nm) with an efficiency dependent upon the inverse 6th power of the donor-acceptor separation. Thus, FRET is a sensitive and direct measure of very close molecular interactions. FRET is manifested in different ways: a decreased donor fluorescence quantum yield, a decreased donor fluorescence lifetime, and an increased stability of the donor towards chemical photobleaching (for references see 28–30). We employed luminescent probes covalently linked to the single terminal amino group of EGF as donor and acceptor molecules. Such extrinsic fluorescent groups, as well as extrinsic protein fluorescence, have been used previously in other studies of the distribution, growth factor binding, internalization, and mechanism of activation of EGFR on living cells or in isolated plasma membranes (9, 23, 26, 27, 42, 59–61). In particular, FRET has been applied in a study of EGFR aggregation on A431 cells and plasma membrane preparations with fluorescent EGF derivatives as donor-acceptor pairs (1, 8, 11). These measurements were based on donor quenching and sensitized acceptor emission for monitoring receptor clustering. Here, we describe experiments on receptor oligomerization using much more sensitive and accurate determinations of FRET based on donor-photobleaching (pbFRET) digital imaging microscopy (28–30) and fluorescence lifetime imaging microscopy (FLIM) (12, 21). The increased sensitivity and accuracy of these methods are due to the application of very sensitive detection devices such as slow-scan CCD-cameras and an image intensifier (FLIM) to high illumination levels combined with long integration times (pbFRET), and the exploitation of temporal phenomena rather than relative fluorescence intensities. Another major virtue of this approach, compared to the use of cells in suspension, is the retention of information related to the spatial distribution of the EGFR. The data confirm that a process of EGF-induced

temperature-dependent receptor dimerization can be visualized on single cells, but the evidence suggests that the high affinity receptor subpopulation is present in an oligomerized state in intact cells, even in the absence of the growth factor ligand. A model is presented in which such preexistent homodimeric complexes are activated by a simple, i.e., nonallosteric, ligand-induced reorientation of the two partners comprising the EGFR dimer. This process is presumed to be transmitted by concerted rotational motions of the transmembrane and cytoplasmic domains, such that the tyrosine kinase domains achieve a stereochemical configuration leading to mutual activation. This mode of stereochemical activation provides an alternative to the mechanism of allosteric receptor oligomerization generally attributed to the large family of growth factor receptors.

## Materials and Methods

### Reagents

Fluorescein-EGF (Fl-EGF) and tetramethyl-rhodamine-EGF (Rh-EGF) were prepared from native-EGF by labeling with FITC and TRITC, respectively, and were purified as described elsewhere (1, 59). Concentrations of native-, Fl-, and Rh-EGF were determined by using molar extinction coefficients $\epsilon_{280}$ = 18,700 $M^{-1}$ $cm^{-1}$, $\epsilon_{493}$ = 73,000 $M^{-1}$ $cm^{-1}$ and $\epsilon_{555}$ = 83,000 $M^{-1}$ $cm^{-1}$, respectively (1, 59). The mAb 2E9 was a kind gift from Dr. Defize (Hubrecht Laboratory Utrecht, The Netherlands). Cell culture reagents were from Cellgro (Herndon, VA) and GIBCO BRL (Gaithersburg, MD). Solvents for spectroscopic measurements were of spectroscopic grade, and other chemicals were of analytical grade.

### Cells and Culture Conditions

A431 human epidermoid carcinoma cells were grown in a 5% $CO_2$ humidified atmosphere at 37°C in DMEM supplemented with 10% FBS, 1 mM sodium pyruvate, 10 mM $NaHCO_3$, 10 mM *N*-tris[hydroxymethyl]methyl-2-aminoethane-sulfonic acid, 10 mM Hepes, 10 mM N,N-bis[2-hydroxyethyl]-2-aminoethane sulfonic acid, pH 7.3, $10^4$ U/L penicillin G and 100 mg/L streptomycin sulfate. After splitting the cells, $2 \times 10^5$ cells were added per petri dish containing medium and seven glass coverslips (20 mm diameter; ~8,000 cells per coverslip). The coverslips were used after 2–3 d.

### Labeling Procedures

Coverslips were transferred to humid incubation chambers (h×w×l = 1×10×15 cm) cooled on ice and washed three times with ice cold PBS. Native-, Fl-, and Rh-EGF were added in various ratios at a total EGF concentration of 50 nM in ice cold PBS supplemented with 50 mM glucose, 5 mM $MgCl_2$, 8.7 mM $CaCl_2$ and 1% (wt/vol) BSA. In the experiments on the high affinity EGF receptors, the cells were preincubated with a ninefold diluted solution of the monoclonal antibody 2E9 (mAb 2E9) (300 nM) in the PBS buffer described above for 4 h at 4°C. After three washes with ice cold PBS, the cells were incubated with EGF as described above. The EGF incubations were carried out for 40 min at 4°C and subsequently at various temperatures and for various times according to the experimental protocol. The coverslips were then washed three times with ice cold PBS and fixed with ice cold 4% (wt/vol) paraformaldehyde in PBS for 5 min, after which the fixation was continued at room temperature for an additional 15 min. Cells were washed twice with PBS, once with a buffer containing 50 mM Tris HCl, pH 7.4, 100 mM NaCl, and mounted in the same buffer on microscope slides within a ring of nail polish to prevent squashing the cells. The preparations were used directly for microscopy after air tight sealing with nail polish.

### pbFRET Fluorescence Microscopy

A Zeiss Axioplan microscope equipped with epi-illumination and fluorescence detection optics was used. The excitation source was an HBO 100 W mercury lamp (Osram, Germany). All images presented here were obtained with a Zeiss Plan-Neofluar 40× NA 1.4 oil immersion objective. Imaging of fluorescein emission (Fl-EGF) was with the filter combination: Zeiss 450–490 nm, excitation; Omega FT 500, dichroic (Omega Optical, Inc. Brattleboro, VT); and Omega 525 DF 30, emission. For collecting the rhodamine fluorescence (Rh-EGF), the filters were: Zeiss BP 546, excitation; Zeiss FT 580, dichroic; and Zeiss LP 590, emission. Image acquisition was with a slow-scan Series 200 (CH220) CCD camera (Photometrics, Tucson, AZ). The camera had a thermoelectrically cooled Kodak KAF-1400 CCD sensor with 1320×1035 (available) 6.8-μm pixels coated with the Metachrome-II down converter. The system was interfaced to an Apple Macintosh IIfx computer via a Photometrics NU200 controller.

The specimens were illuminated constantly and a sequence of fluorescence micrographs (usually 31, each 7.5–10 s in duration) was acquired with the CCD camera. Successive micrographs (subimages) exhibited decreasing intensities with time due to the photobleaching process. After exporting the data to a DEC MicroVax II computer, a pixel-by-pixel single exponential decay (DECAY program, (30); Gadella, T. W. Jr., and T. M. Jovin, manuscript in preparation) was fit to the sequence of subimages, thereby providing images of the photobleaching amplitudes and time constants, the residual background intensities and other information. The FRET efficiency E (range 0–1) was calculated from the photobleaching time constants of the FRET-donor obtained in the absence ($\tau_{bl}$) or presence ($\tau'_{bl}$) of the FRET-acceptors according to

$$E = 1 - \frac{\tau_{bl}}{\tau'_{bl}} \quad (1)$$

In a two state model accounting for only two populations of receptors, either in a monomeric or in a dimeric state, it can be shown that the minimal amount of receptor dimerization ($\alpha_{min}$) is related to E and the fraction of acceptor labeled EGF (relative to the total amount of added EGF) $f_A$ according to Eq. 2 (see also Appendix).

$$\alpha_{min} = \frac{8E}{f_A(2+E)^2} \quad (2)$$

### Fluorescence Lifetime Imaging Microscopy

The frequency domain fluorescence lifetime imaging microscope has been described in detail (12, 21). Briefly, the microscope consisted of an epi-illumination Zeiss Universal Microscope (Oberkochen, FRG), coupled to an image intensifier-CCD detection system. The excitation source was the 488-nm line of an argon-ion laser modulated with acousto-optical modulators. After passing through a quartz optical fiber (0.2 mm diameter, several meters in length), the central (zero order) diffraction spot was directed into the side port of the microscope epi-illuminator. The image intensifier (PCO Computer Optics GmbH, Kelheim, FRG), consisted of a microchannel-plate (MCP) intensifier, a S20 photocathode gateable down

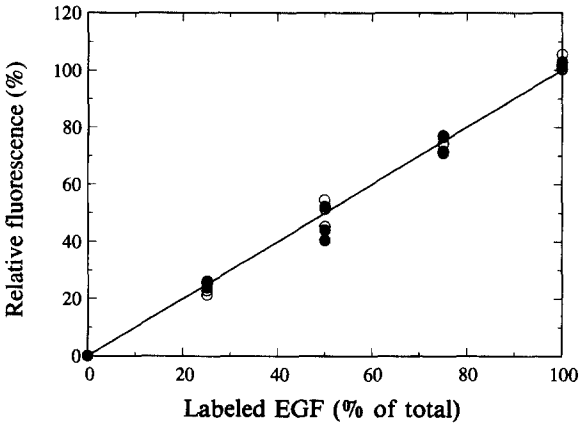


*Figure 1.* Competitive binding of native-, Rh-, and Fl-EGF. A431 cells were incubated with 50 nM EGF (total concentration) as described with various ratios of Fl-EGF/native-EGF (○) or Rh-EGF/native-EGF (●). After labeling for 40 min at 4°C, the cells were fixed and used for microscopy as described. The relative average fluorescence intensity from three representative groups of cells is plotted against the labeling ratio.

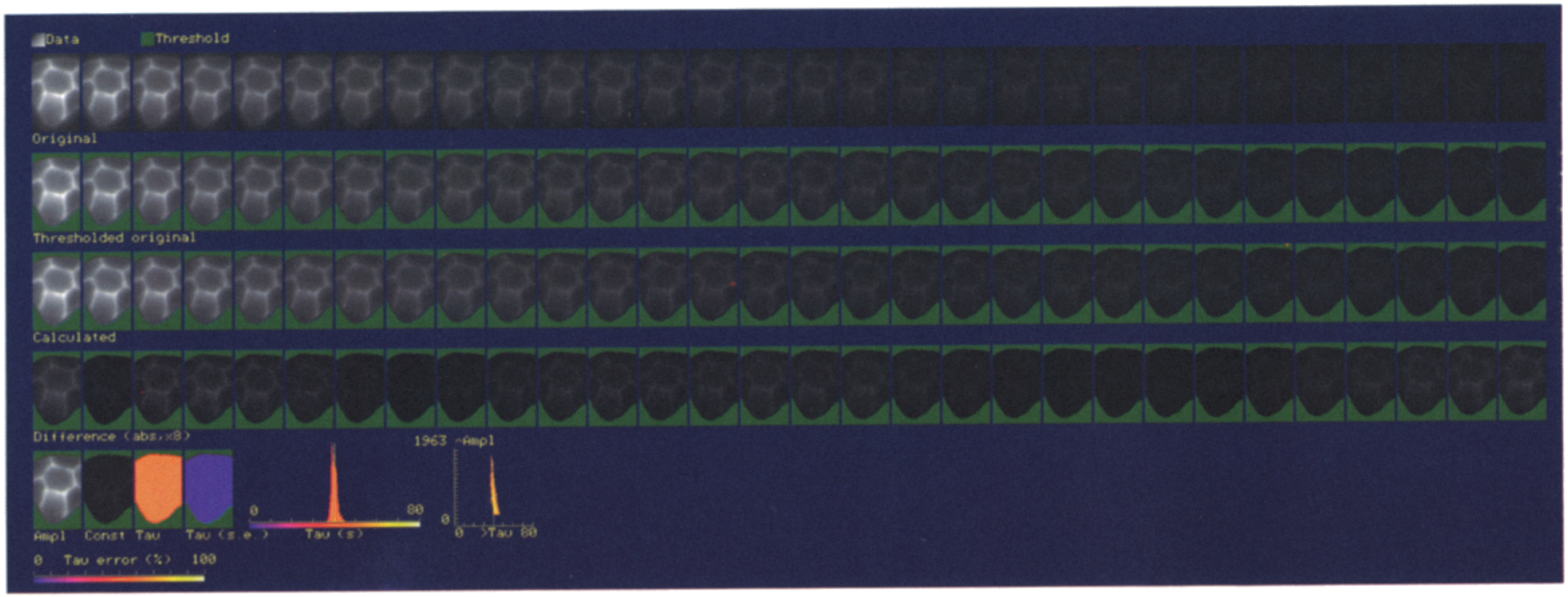


*Figure 2.* Photobleaching FRET microscopy of Fl-EGF bound to A431 cells were labeled with 16.7 nM Fl-EGF and 33.3 nM native EGF at 4°C for 40 min and then for 5 min at 20°C. The cells were then fixed and mounted as described. A sequence of 31 fluorescence micrographs combined together in one image was taken with the CCD camera. The first (a dark image) was acquired with the excitation shutter closed and the others by opening the shutter for 7.5 s. The digital image sequence was transferred to the DEC Micro Vax II and analyzed with the DECAY program. The generated output was image processed by use of a TCL-Image macro yielding the final displayed image. For further details see Materials and Methods.

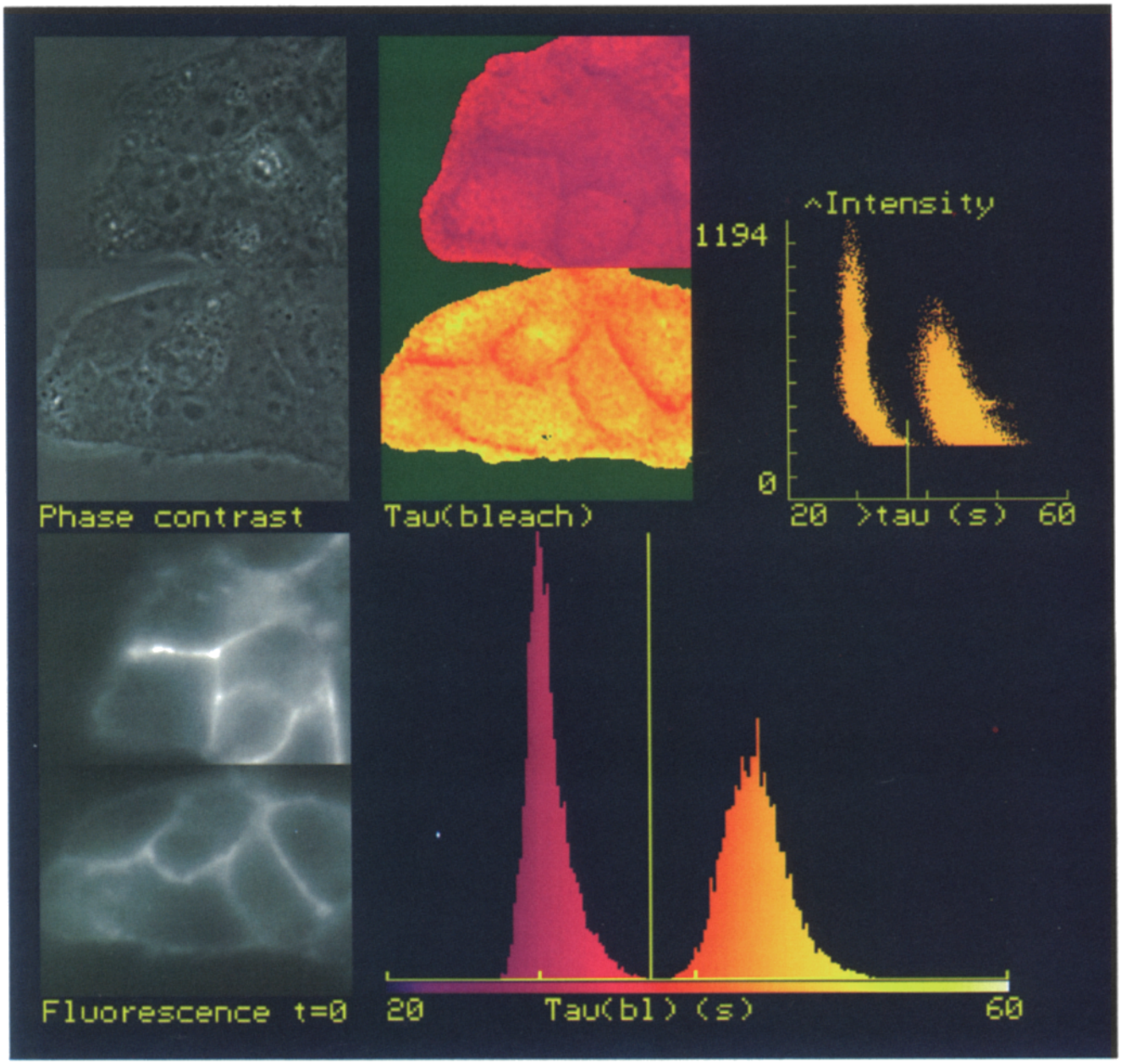


*Figure 3.* pb-FRET microscopy of Fl-EGF and Rh-EGF bound to A431 cells after a 5-min exposure to 37°C. A431 cells were labeled with 16.7 nM Fl-EGF and either 33.3 nM native-EGF (*top images*) or 33.3 nM Rh-EGF (*bottom images*) at 4°C for 40 min and then for 5 min at 37°C. The cells were then fixed and mounted as described. Two sequences (one per labeling condition) of 21 fluorescence micrographs were acquired by the CCD camera, using a shutter open time of 11 s. Corresponding phase contrast images were also taken. The digital sequence images were transferred to the DEC MicroVax II and merged together in one sequence by use of a macro written in TCL-Image. This sequence image was analyzed as in Fig. 2. The standard output of the DECAY program was modified with TCL-Image in order to generate a more compact output comprised of: phase contrast images of the cells (*top left*), the initial fluorescence images (*bottom left*), the $\tau_{bl}$ images (*top middle*), the $\tau_{bl}$ temporal histogram (*bottom middle*), and the two-dimensional $\tau_{bl}$ vs Ampl. histogram (*top right*). For the average image statistics (Table I), the two sequences were also analyzed separately.

to ~5 nsec, a P46 phosphor, and provision for a high frequency (HF) modulation input directly at the high voltage MCP stage. The HF driving current was provided by a power amplifier driven at a frequency 40 Hz (= $\Delta f$) higher than that of the AOMs. The CCD camera system (Photometrics Series 200, Tucson, AZ) incorporated a mechanical shutter and a thermoelectrically cooled CSF-Thomson 7882(1)A CCD sensor of 576×384 23×23 μm square pixels with a Metachrome II down converter coating to boost the blue sensitivity. The camera controller was interfaced to an Apple Macintosh IIci computer and operated with a dedicated acquisition program implemented with LabView (National Instr., Austin, TX).

The donor (fluorescein) fluorescence was collected with a Zeiss FT 505 dichroic mirror and a Zeiss PB 520–540-nm emission filter. The sequence of phase images was acquired using the heterodyne "boxcar" mode of measurement (20, 21). One phase image was obtained by applying a gate of 4 ms to the cathode of the MCP intensifier at one particular phase setting of the low frequency ($\Delta f$) signal, and integration of the ensuing signal on the phosphor screen of the MCP intensifier for 2 s on the CCD. Twenty images were recorded by gating the fluorescence signal at time delays varying from 0–18 ms within the 40 Hz heterodyne cycle. The first 10 images were obtained by increasing the time delay with steps of 2 ms and the

*Table I. Average Parameters from Photobleaching Experiments*

| Temperature °C | Acceptor* yes/no | $\tau_{bl}$ | E‡ | CV§ | s.e.‖ | N¶ |
|---|---|---|---|---|---|---|
| | | *s* | % | % | *s* | |
| 4 | no | 39.8 | – | 6 | 1.2 | 6998 |
| 4 | yes | 41.7 | 4.6 | 4 | 1.5 | 7311 |
| 20 | no | 40.3 | – | 4 | 0.9 | 6195 |
| 20 | yes | 46.8 | 14 | 3 | 1.0 | 3701 |
| 37 | no | 30.6 | – | 5 | 1.7 | 21687 |
| 37 | yes | 44.1 | 31 | 5 | 1.6 | 20513 |
| 4 | no | 39.6 | – | 6 | 1.7 | 7920 |
| 4 | yes | 41.4 | 4.3 | 4 | 1.7 | 7920 |
| 4** | no | 43.2 | – | 6 | 2.7 | 7920 |
| 4** | yes | 60.2 | 28 | 12 | 4.6 | 7920 |

* Presence/absence of acceptor. *No*, incubation with Fl-EGF/native-EGF = 1:2; *Yes*, incubation with Fl-EGF/Rh-EGF = 1:2.
‡ Effective average energy transfer calculated from Eq. 1.
§ Coefficient of variation in $\tau_{bl}$ (100 × SD/mean, all pixels).
‖ Average standard error per individual $\tau_{bl}$ determination.
¶ Number of analyzed pixels (single exponentials), in all cases the average correlation coefficients were ~99.2% and the average residuals (= $\Sigma$[observed - calculated]$^2$/$\Sigma$observed$^2$) were ~5%.
** With added 2E9 monoclonal antibody.

last 10 by decreasing the time delay in 2 ms steps. By addition of the digitized intensities of the images with equal time delay, photobleaching effects (up to a maximal 20%) were corrected (21). The phase shift ($\Delta\Phi$) and modulation (M) were determined at every pixel from the series of images relative to that of scattered excitation light using the fit program SINUS (20). The overall fluorescence lifetimes ($\tau_\Phi$ and $\tau_M$) were calculated according to Eqs. 3 and 4 using $2\pi \cdot 39.19 \cdot 10^6\ s^{-1}$ as the radial frequency $\omega$.

$$\tau_\Phi = \frac{1}{\omega}\tan(\Delta\Phi) \tag{3}$$

$$\tau_M = \frac{1}{\omega}\sqrt{\frac{1}{M^2} - 1} \tag{4}$$

## Results

### Relative Affinities of Fl-, Rh-, and Native-EGF

The relative affinities of Fl- and Rh-EGF compared to that of native-EGF were investigated by studying the fluorescence intensity of the labeled compounds bound to A431 cells upon dilution with native-EGF (Fig. 1). As can be inferred from the very linear relationships of relative fluorescence intensity and the fractional contribution of labeled EGF added to the A431 cells, the affinities of Fl- and Rh-EGF were very similar to that of native EGF. A similar conclusion was reached by others (1, 8).

### pbFRET Microscopy of Fl-EGF

A typical donor photobleaching experiment of Fl-EGF bound to A431 cells is shown in Fig. 2. The figure is a composite graphical output produced by the fit program DECAY and image-processing in TCL-Image as described in Gadella, T. M. Jr., and T. M. Jovin (manuscript in preparation). The first row of subimages depicts the original CCD camera data. The second row shows the same data after thresholding, such that low intensity points outside the cells are masked. The third row depicts the calculated data based on the single exponential fit through (all) original images. The accuracy of the fit can be estimated from a comparison of the second and third rows and with greater resolution in the fourth, which depicts the differences between the original and calculated data (multiplied by 8). The fifth row shows the bleachable fraction of the initial fluorescence (Ampl image), the nonbleachable part (Const. image), the photobleaching time constant image $\tau_{bl}$ (Tau) and the image of its relative estimated S E. Also included are a histogram of the photobleaching time constants and a two dimensional histogram of $\tau_{bl}$ vs the Ampl. image which shows the correlation between fluorescence intensity and photobleaching kinetics. As can be seen from the very narrow distribution of $\tau_{bl}$, the bleach kinetics were very similar on different parts of the cells. For the FRET experiments, the standard output of the fitting program was modified to include a phase contrast image of the cells, the initial fluorescence image, the $\tau_{bl}$ image, the $\tau_{bl}$ temporal histogram, and the two-dimensional $\tau_{bl}$ vs Ampl. histograms (Figs. 3–5). The average statistics in Table I show a very large correlation coefficient, low residuals, and small standard deviations, attesting to the good quality of the experimental data.

### Effect of Temperature on EGFR Dimerization Determined by pb-FRET Microscopy

In the pbFRET experiment depicted in Fig. 3, the photobleaching times were compared for cells labeled with Fl-EGF/native-EGF = 1:2, (donor in absence of acceptor, top images) with those of cells labeled with Fl-EGF/Rh-EGF = 1:2 (donor in presence of acceptor, lower images). The incubation with EGF before fixation was for 40 min at 4°C and then for 5 min at 37°C. It can be clearly seen that the photobleaching time constants were higher for the cells labeled with Fl- and Rh-EGF than those for the cells labeled with Fl- and native-EGF. This difference was due to FRET arising from receptor dimerization/oligomerization. Even though the warming periods were very brief, it is likely that some internalization due to receptor-mediated endocytosis took place, particularly at 37°C. From the quite homogeneous color (i.e., photobleaching rate) of the $\tau_{bl}$ images, however, it appears that the FRET efficiency was not correlated with certain cell structures. This homogeneity can also be inferred from the narrow $\tau_{bl}$ histograms and from the low average coefficients of variation (<CV>) of 7–8% for both labeling conditions (see Table I, in which other average image statistical parameters are also listed). From the average $\tau_{bl}$'s, we estimated an effective transfer of 31%, a value consistent with a minimal receptor dimerization of ~70% within the two compartment state model (Eq. 2).

Similar experiments were performed at different temperatures. Fig. 4 shows the result of a 5-min warming to 20°C after equilibrium binding at 4°C, whereas Fig. 5 depicts the comparison data obtained without such a warming period (control). The presence of FRET in Fig. 4 is apparent from the difference in the $\tau_{bl}$ images. There was no obvious correlation between $\tau_{bl}$ and cellular structures. In Fig. 5, however, the color in both $\tau_{bl}$ images is nearly identical implying a low FRET efficiency E. As can be inferred from the various average $\tau_{bl}$ (see Table I), the average value of E decreased with temperature (31, 14, and 4.6% at 37, 20, and 4°C, respectively). According to a two-com-

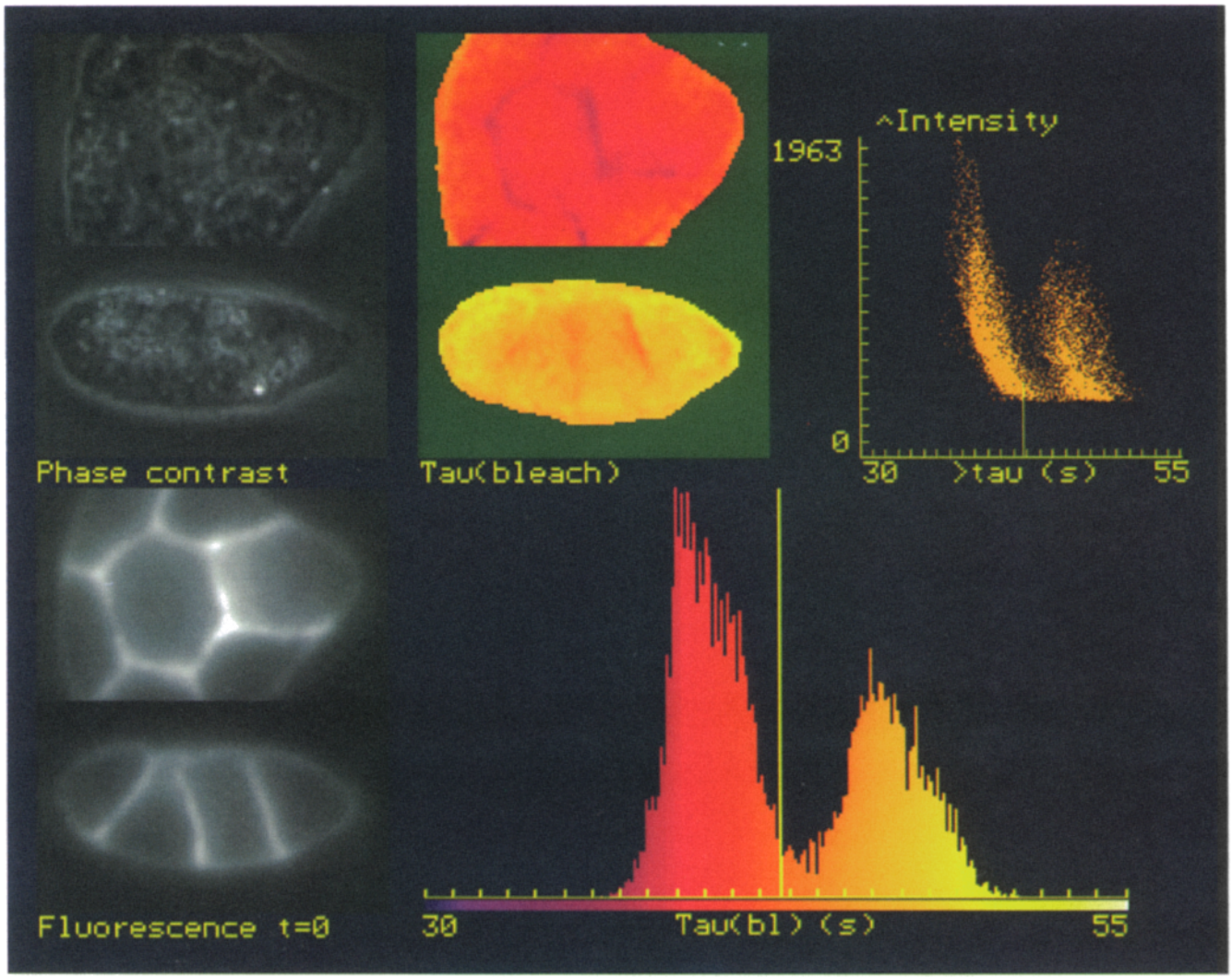


*Figure 4.* pbFRET microscopy of Fl-EGF and Rh-EGF bound to A431 cells after a 5-min exposure to room temperature. Cells were labeled as described in the legend to Fig. 3 but exposed to a warming period of 6 min at 20°C. Two sequences of 31 fluorescence micrographs were acquired by the CCD camera, with a shutter open time of 7.5 s. Two phase contrast images were also taken. Subsequent image analysis and processing was as described in Fig. 3.

partment state (single and dimerized) receptor model (Eq. 2), the minimal average percentage of dimerization was 69% at 37°C, 36% at room temperature, and only 13% at 4°C. These results are indicative of a global, temperature-dependent dimerization process within 5 min after EGF binding to the receptor.

### *EGF Dimerization Studied by FRET-FLIM*

The new technique of fluorescence lifetime imaging microscopy (FLIM) directly determines the fluorescence lifetimes on single cells (21) and thereby is the most direct technique available to quantitate FRET in cellular systems. The method has been described in detail elsewhere (21). The standard output as described in that paper was modified in order to reproduce the two separate experiments (Fl-fluorescence in the presence and absence of Rh) in one figure. The result of such a FLIM experiment is shown in Fig. 6. As expected, the fluorescence lifetime was reduced for the double-labeled cells in comparison with single-labeled ones. This can be seen from the more bluish color in the $\tau'_\Phi$ image compared to the $\tau_\Phi$ image and from the shift to the left of the $\tau_\Phi$ distribution histogram. The same holds for $\tau_M$. From the average $\tau_\Phi$, we determined a transfer efficiency of 16% and from $\tau_M$ of 11% (see also Table I). These values compare favorably with those in Fig. 4. The difference between the effective FRET efficiency determined with the different techniques results from different weighing of the data (see discussion below). The distributions of $\tau_\Phi$ and $\tau_M$ are broader than the ones depicted in Fig. 4, due to the smaller number of sequence images taken and the lower statistical significance.

### *Effect of mAb 2E9 on FRET Efficiency at Low Temperature*

To estimate the oligomerized state of the high affinity EGF receptors on A431 cells, photobleaching experiments were performed on cells preincubated with the monoclonal antibody mAb 2E9. This antibody specifically blocks the sub-

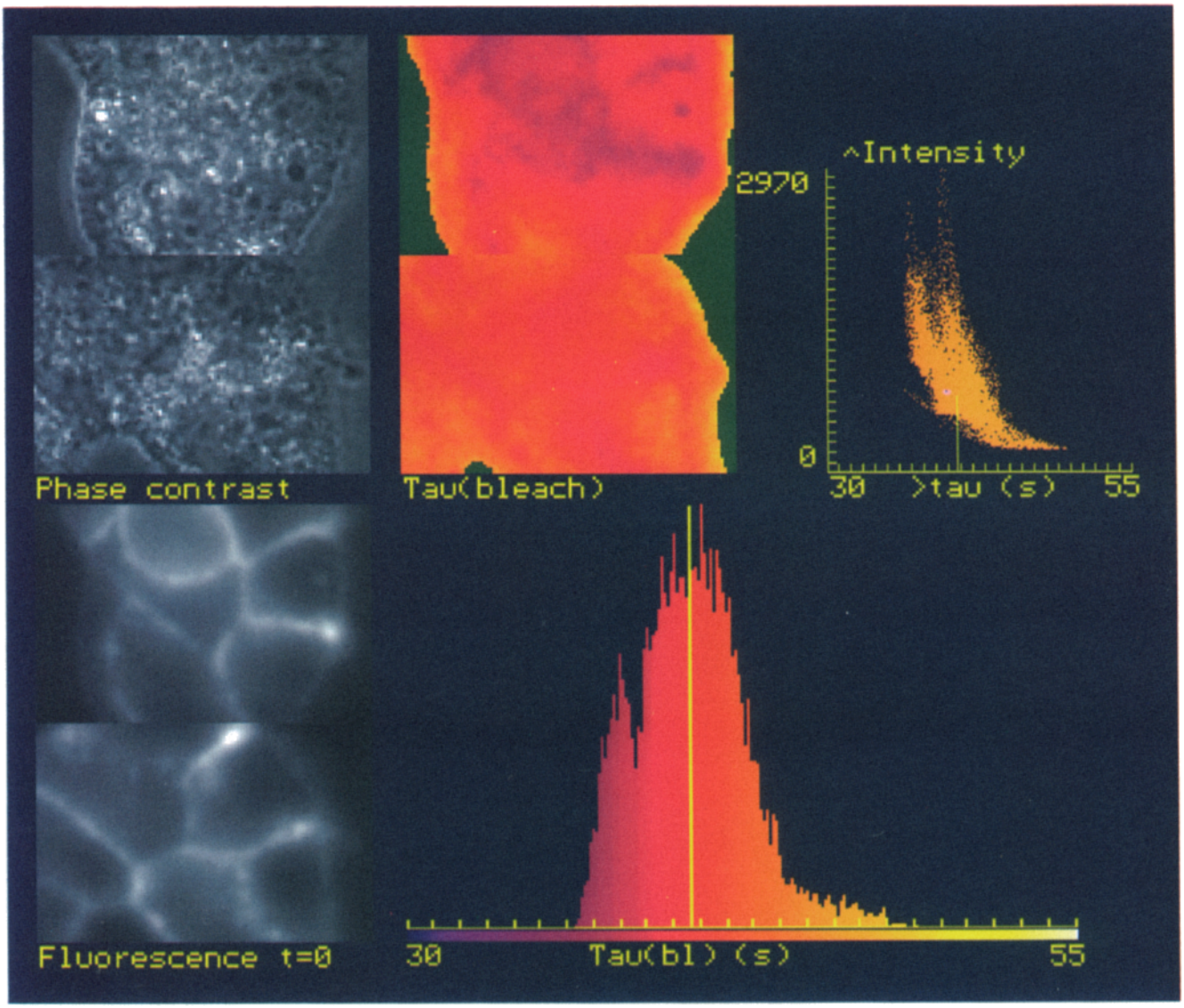


*Figure 5.* pbFRET microscopy of Fl-EGF and Rh-EGF bound to A431 cells after incubation at 4°C. A431 cells were labeled as described in Fig. 3, however, the 5 min incubation at 37°C was canceled. Two sequences of 51 fluorescence micrographs were acquired by the CCD camera, the first image in both sequences with the excitation shutter closed (*blank*) and the others by opening the excitation shutter for 7.5 s each. Also two phase contrast images were acquired. Subsequent image analysis and processing was as described in the legend to Fig. 3.

population of low affinity EGFR (15). The results of this experiment are summarized in Fig. 7. The control incubations showed a similar effect to that described in Fig. 5. After preincubation with mAb 2E9, the overall fluorescence labeling was clearly reduced (more than fivefold) reflecting the blocking of >80% of the EGF-binding sites. Although the bleaching kinetics of Fl-EGF (donor alone) were essentially unchanged, a large increase in $\tau_{bl}$ was observed in the double-labeling experiment. This result is in dramatic contrast to that achieved in the control experiment without the mAb 2E9. An average FRET efficiency of 28% was estimated, corresponding within the two-state model to a ≥65% dimerization of the high affinity EGFR. In the regions of intercellular contact, $\tau'_{bl}$ was lower (Fig. 7). These regions also exhibited a relatively high fluorescence intensity. We infer from these results that the EGFR in the plasma membranes involved in cell–cell contact was less accessible to the mAb 2E9 antibody. A transfer efficiency

*Figure 6.* FRET-FLIM of Fl- and Rh-EGF bound to A431 cells after a 6-min exposure to room temperature. Cells were labeled as described in the legend to Fig. 4. For the FLIM measurement 20 phase images were acquired for each labeling condition at an HF of 39.19 MHz (see Materials and Methods). These images were transferred to a MicroVax II system and analyzed by the SINUS program (20, 21) and image processed with TCL-Image. The displayed image was generated by copying selected areas from the final TCL with the program NIH-Image (National Institutes of Health, Bethesda, MD). Text was added with Canvas (Deneba Software, Miami, FL). The

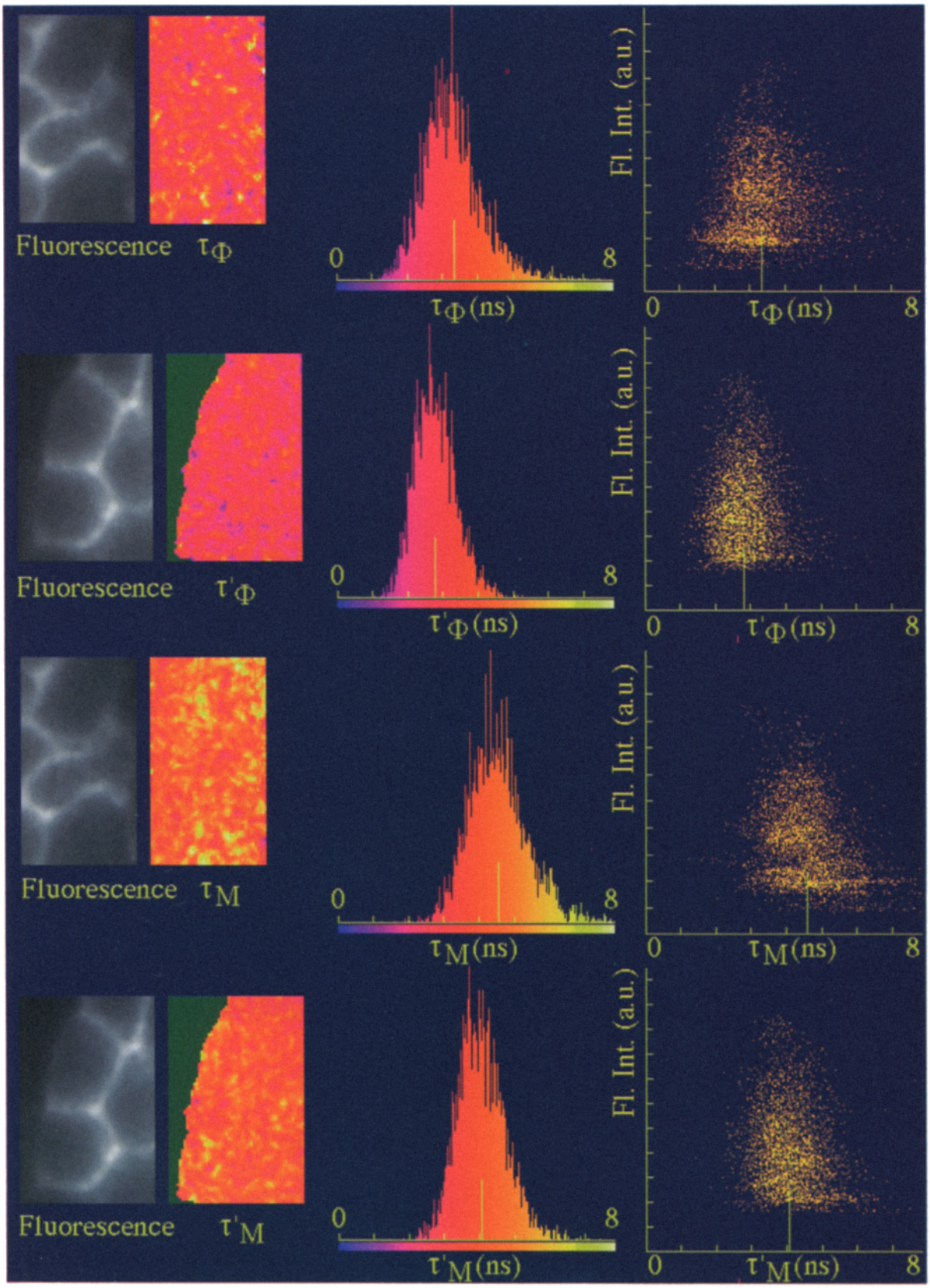


image consists of three columns. The first column depicts from top to bottom: an original phase image (*left*) and the corresponding $\tau_\Phi$ image (*right*) of cells labeled with Fl-/Native-EGF = 1:2; an original phase image plus corresponding $\tau'_\Phi$ image of cells labeled with Fl-Rh-EGF = 1:2; and similar images combining the $\tau_M$ and $\tau'_M$ (*lower two*). The second column shows the temporal distribution of the colored lifetime images in the first column, and the third column depicts the two-dimensional histograms showing the correlation between the fluorescence intensity (*left half of the first column*) and the fluorescence lifetimes (*right half of first column*).

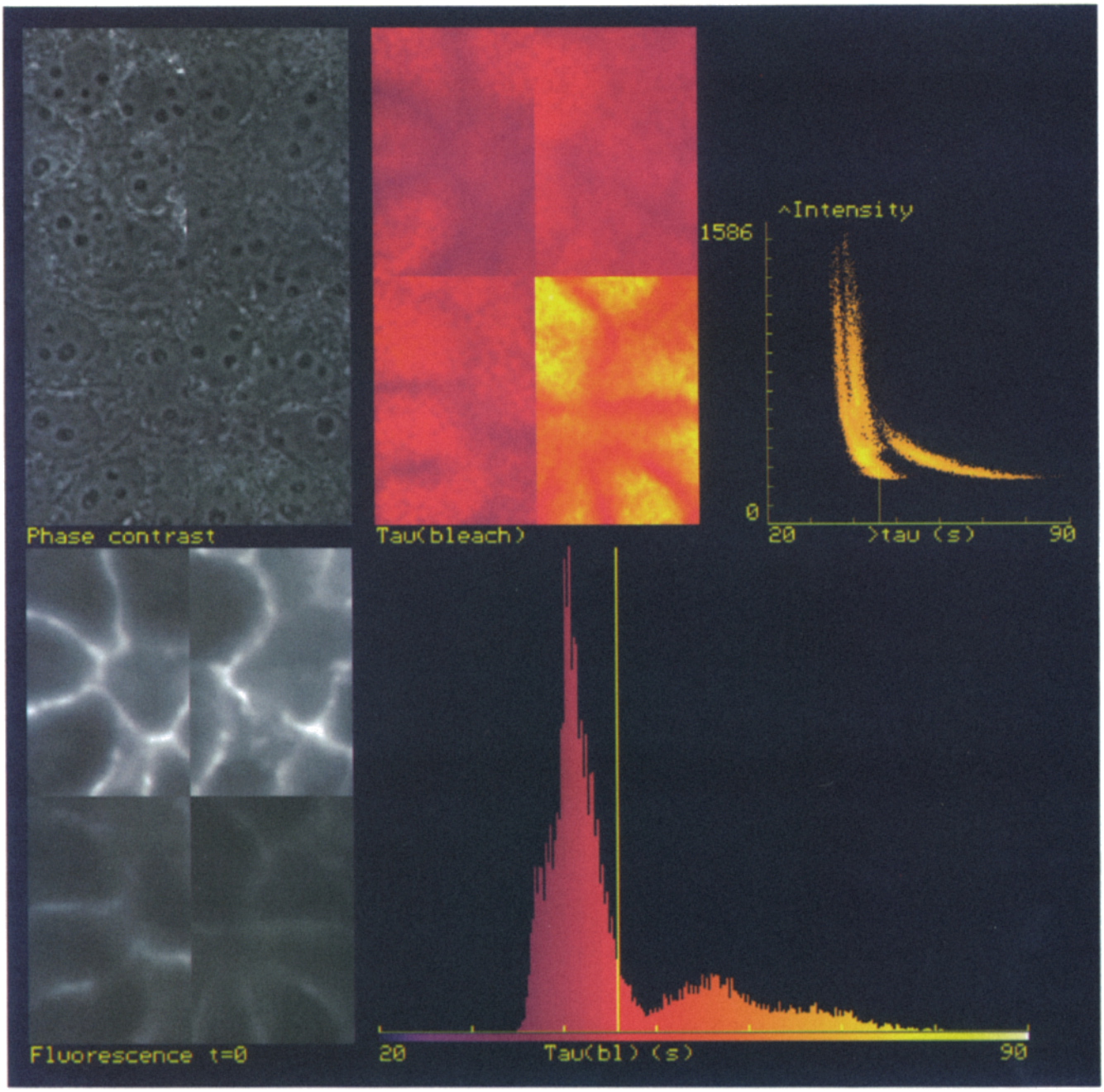


*Figure 7.* Effect of mAb 2E9 on the photobleaching kinetics of Fl-EGF in the presence and absence of Rh-EGF, both bound to A431 cells. A431 cells were pretreated with (*lower half images*) or without (*upper half images*) 300 nM mAb 2E9 for 4 h at 4°C as described. Then 16.7 nM Fl-EGF and either 33.3 nM native EGF (*left half images*) or 33.3 nM Rh-EGF (*right half images*) was added to the cells for 40 min at 4°C. Further image processing was as described above.

(E) image (Fig. 8 *A*) was obtained by processing the lower right section of the $\tau_{bl}$ image in Fig. 7 by use of Eq. 1. It is apparent from Fig. 8 that some regions exhibited a much higher (and the intercellular regions a much lower) transfer efficiency than the average 28%. By subsequent application of Eq. 2, Fig. 8 *A* was transformed into an $\alpha_{min}$ image (Fig. 8 *B*, and as a pseudo three-dimensional representation in Fig. 8 *C*) displaying the minimal percentage of

*Figure 8.* Quantitation of FRET efficiency and minimal receptor dimerization of the high affinity EGF receptor subclass of A431 cells labeled with Fl- and Rh-EGF. By using $<\tau_{bl}>$ = 43.32 s from the bleach experiment of Fl-/Native-EGF = 1:2 in the presence of mAb 2E9 (Fig. 7, *bottom left images*; Table I) the $\tau'_{bl}$ image of the experiment with Fl-EGF/Rh-EGF = 1:2 in the presence of mAb 2E9 (Fig. 7, *bottom right images*) was processed according to Eq. 1 to yield an E (*transfer efficiency*) image (*A*). By application of Eq. 2, this image was further processed to yield an $\alpha_{min}$ image (*B*). *C* is a pseudo-3D representation of *B*.

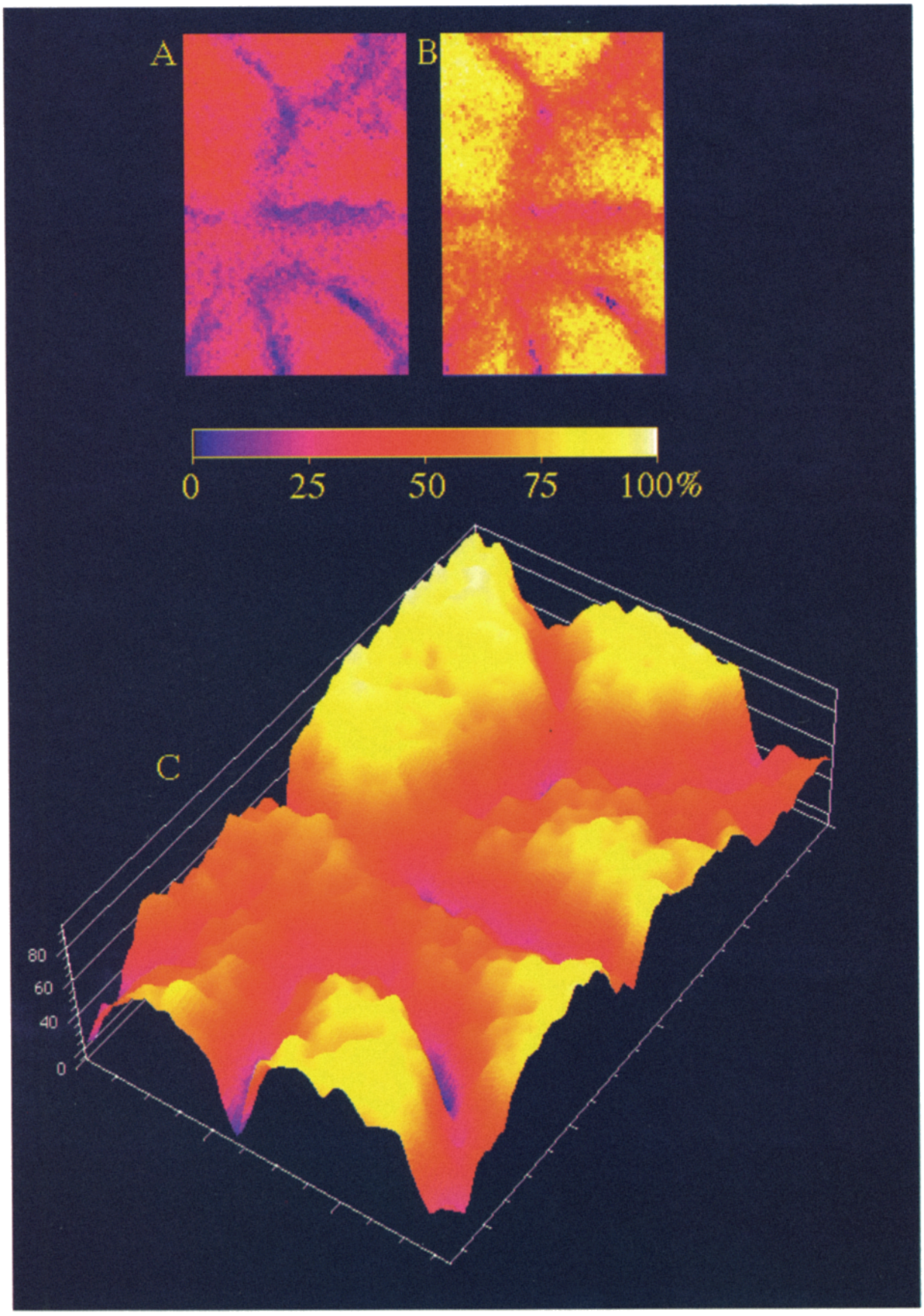


*Figure 8.*

dimerized receptors in a spatially resolved manner. From Fig. 8, *B* and *C* and within the context of a two-state mode, it is apparent that the (high affinity) population of EGFR resistant to blockage by mAb 2E9 was dimerized up to 100%.

## Discussion

In this study we investigated EGF receptor microclustering on single cells by use of FRET-microscopy techniques. The application of FRET in previous studies of EGFR microclustering was restricted to suspensions of intact cells or isolated plasma membranes (1, 8, 11) or to studies of the soluble, extracellular domain of EGFR (58). In these investigations, FRET was estimated from donor quenching (1, 8, 11) or sensitized acceptor emission (1). The major advantage of kinetic parameters (photobleaching time constants or fluorescence lifetimes), as opposed to steady-state emission signals, is that they are independent of labeling efficiencies, relative affinities, or steady-state background contributions (28–30). In this respect it is interesting to focus on the results described in references 1, 8, and 11. Azevedo and Johnson incubated isolated plasma membranes with Fl-EGF/Rh-EGF = 1:2; Fl-EGF/native-EGF = 1:2; or native-EGF:Rh-EGF = 1:2. After incubation the unbound EGF was removed by pelleting the membranes and subsequent resuspension. The energy transfer was estimated from comparison of the fluorescence emission spectrum of the membranes labeled with Fl-EGF/Rh-EGF = 1:2 with that of a mixture of the other membranes. From the sensitized emission they estimated a transfer efficiency of 21% at 37°C but in the same spectrum, donor quenching was only 6%. The authors explained the discrepancy by slight changes in the absorbance spectrum of Fl- and Rh-EGF after binding to the receptor, which can have a large effect on the calculation of sensitized emission. Although we did not observe differences in the affinities of Fl-, Rh-, and native-EGF for the receptor (Fig. 1), changes on the order of 5–10% due to the introduction of the external probe cannot be excluded. Such differences would produce major errors (>100%) in the steady-state measurements of FRET described above. The alternative approach of Carraway and colleagues was to first label cells (or membrane preparations) with Fl-EGF and then titrate with EGF labeled with eosin-isothiocyanate (E-EGF) while monitoring the quenching of Fl fluorescence. According to this approach Fl-EGF would first occupy all the oligomerized (high affinity) sites, after which binding of E-EGF would be incapable of eliciting energy transfer. With intact cells, Carraway and colleagues indeed failed to find energy transfer with this method (8), whereas with isolated membranes they detected up to 20% energy transfer depending on the labeling conditions (8, 11). In an effort to circumvent the problem posed by sequential additions, they added the labeled proteins simultaneously but obtained essentially the same results. We note that simultaneous addition poses two new problems in such experiments: (*1*) there is no discrimination between bound and unbound EGF; and (*2*) any difference in relative affinities can introduce artifacts (see above).

With time-resolved techniques, we were able to determine FRET on single, attached, viable cells and demonstrated a temperature-dependent rapid microclustering of EGF receptors. The approach described here has the advantage that no further control experiments need to be performed, inasmuch as the difference in Fl-EGF photobleaching kinetics or fluorescence lifetime can only be due to the presence or absence of Rh-EGF. Changes in quantum yield or absorption coefficients upon binding of the EGF-derivatives to the receptor are irrelevant for time-resolved determination of FRET since only the receptor-bound fraction is monitored. Slight differences in affinity can proportionally change steady-state relative intensities but do not interfere with the determinations of photobleaching kinetics or fluorescence lifetime of Fl-EGF bound to receptor monomers, although they can of course influence the ratio of donor-to-acceptor labeling, causing it to deviate from the reagent ratio. The latter effect would influence the FRET efficiencies but not the accuracy of their estimation. For the interpretation of the transfer efficiencies in terms of a lower limit for receptor dimerization a labeling ratio of 1:2 was assumed ($f_A = 2/3$ in Eq. 2).

The low temperature incubation (4°C for 40 min, see Fig. 5) revealed donor photobleaching kinetics similar in the presence and absence of acceptor under control situations. Such experiments rule out possible procedural artifacts like fixation induced receptor clustering. A 6-min warming period to room temperature after low temperature binding of EGF caused a substantial increase in $\tau_{bl}$ (Table I, Fig. 4), which was accompanied by a decrease in fluorescence lifetime (Table II, Fig. 6). Both parameters were indicative of energy transfer. Given the critical transfer distance $R_o$ for Fl-EGF to Rh-EGF FRET of 5.3 nm (1) energy transfer can only occur if the receptors are very close together. From the average transfer efficiency of 31% after a 5-min warming period to 37°C, we could conclude that the maximal distance between Fl- and Rh-EGF in a dimerized receptor is ~5 nm, assuming a two state monomer/dimer model (unpublished data). In a dual cylinder model of the EGF-receptor dimer, with an EGF molecule bound in the center of each cylinder, this would imply that the maximal diameter/length ratio of each EGFR monomer is ~0.5 (assuming a molecular mass of 170 kD and a density of 1.2 g/cm$^3$). This ratio is indicative of an elongated receptor structure, allowing many contacts between the adjacent receptor monomers.

EGF-induced dimerization of the EGFR is a general phenomenon that has been described using a variety of techniques (see also introduction). With purified recep-

*Table II. Mean Parameters from FLIM Experiments*

| Acceptor* | $\tau_\Phi$ | CV‡ | s.e.§ | $tau_M$ | CV‡ | s.e.§ | N¶ |
|---|---|---|---|---|---|---|---|
| | *ns* | % | *ns* | *ns* | % | *ns* | |
| no | 3.3 | 27 | 0.8 | 4.6 | 19 | 0.8 | 3946 |
| yes | 2.8 | 22 | 0.6 | 4.1 | 17 | 0.7 | 3738 |

* Presence/absence of acceptor. *no*, incubation with Fl-EGF/native-EGF = 1:2; *yes*, incubation with Fl-EGF/Rh-EGF = 1:2.
‡ Coefficient of variation in $\tau$ (100 × SD/mean, all pixels).
§ Average standard error per individual $\tau$ determination.
¶ Number of analyzed pixels (sine waves). In both cases the average correlation coefficients were ~97% and the average residuals (= $\Sigma$[observed - calculated]$^2$/$\Sigma$observed$^2$) were ~3%.

tors, ligand-dependent dimerization was demonstrated by nondenaturating gel electrophoresis and by density gradient centrifugation (3, 56, 57). Studies on intact cells have been limited to spectroscopic or microscope-based techniques using labeled EGF. In addition to FRET, time-resolved phosphorescence anisotropy has been used to monitor the microclustering of EGFR in cells and in membrane fragments (59–61). It was found that the rotational diffusion of receptor-bound EGF was slower at high temperature (37°C) than at low temperature (4°C), in agreement with our results. Other nonmicroscope techniques applied to cells have made use of chemical cross-linkers in combination with electrophoretic techniques to demonstrate the dimerized receptor. Despite the manifest utility of chemical cross-linking, it is accompanied by a number of pitfalls and artifacts (for an overview see reference 47). First, the method is highly specific in that hetero-associations of EGFR with other proteins are scored (17). This effect will be even more pronounced on permeabilized cells or on plasma membrane preparations. Second, some cross-linking agents can diffuse through plasma membranes of intact cells and hence cross-link already internalized receptors, such as those bound to elements of the cytoskeleton (17). Third, the yield of cross-linking can never achieve 100%, leading to a systematic underestimation of the fraction of dimerized receptor (13). Some of these problems can be circumvented by appropriate control experiments, but we would rather emphasize the comparative virtues of the time-resolved fluorescence microscope techniques used in the present study: (*a*) they are highly sensitive and labeling is highly specific. (*b*) They produce spatial resolved information on single cells. (*c*) Perturbation of the system is minimal such that living cells can be studied (59). (*d*) The information obtained is very direct such that data interpretation is straightforward, allowing even a quantitative estimation of receptor dimerization.

An intriguing and not yet completely resolved question concerns the oligomerized state of the high affinity receptor. Many studies have pointed to a linkage between high affinity EGF binding, cellular activation, and receptor dimerization (see Introduction). In some cases, the EGF concentration was varied in order to specifically label the high affinity receptor. In a previous study it was determined that 12% of the EGF receptors have high affinity sites ($K_d$ = 0.7 nM) and 88% of the EGF receptors have low affinity sites ($K_d$ = 36 nM) on A431 cells (59). High affinity sites were selected by addition of only 3 nM EGF whereas the total population was selected by addition of 110 nM EGF. In these two situations it can be shown that the ratio of high affinity to total binding would have been 59% and 15%, respectively. In the present study the monoclonal antibody 2E9 (15) was used to discriminate the high and low affinity receptors. This antibody essentially blocks low affinity EGF sites (15) and thereby provides a very specific tool for studying high affinity receptors. Interestingly, another monoclonal antibody has been described that specifically inhibits high affinity EGF-binding (2). Using mAb 2E9, we could demonstrate a significant FRET efficiency between Fl- and Rh-EGF at 4°C, whereas in the absence of the antibody very low efficiencies were obtained (Fig. 7). At 4°C, EGF-receptor patch-formation and receptor-mediated endocytosis are completely inhibited (4, 13, 22, 25, 40, 54), and hence the observed increase in transfer efficiency can only be explained in terms of microclustering or dimerization. Considering the substantial number of publications reporting on an EGF-receptor dimer (3, 13, 17, 18, 40, 45, 46, 56–58), we interpret the observed transfer efficiencies in terms of receptor dimerization rather than generalized oligomerization. Applying a quantitative evaluation based on a two-state model, we have concluded that receptor dimerization was close to 100% in some regions of A431 cells treated with mAb 2E9 (Fig. 8). This result strongly suggests that the high affinity EGF receptor is present in a dimerized state. Since high affinity receptors can be activated by EGF (15) receptor dimerization per se may not necessarily lead to receptor activation. Rather, we favor the hypothesis of Spaargaren et al. (46) that the high affinity subclass consists of receptors in an intermediary inactive state which can be fully activated only upon EGF binding. We propose a model in which both receptor monomers undergo a relative rotation in response to the stereochemical interaction between two binding EGF molecules (Fig. 9). This motion is transmitted to the cytoplasmic domains of the two EGFR monomers, bringing them into a relative configuration favorable for activation of the tyrosine kinase (32). Such a "frozen" dynamic dimer model has been proposed for transmembrane signaling via receptors involved in bacterial chemotaxis (31). There are no allosteric features in this 'twist' mechanism, inasmuch as a conformational transition of the macromolecular species influencing ligand-binding affinity is not required. It also provides the means for circumventing the difficulties encountered in theoretical treatments of the binding-dimerization linkage paradigm (55). One can, for example, postulate that the enhanced affinity of the EGFR dimer for the growth factor, a characteristic feature of the TKR systems, arises from a hybrid-binding site comprising the primary binding locus on each monomer and a secondary interaction site or sites on the second monomer. The proposed mechanism does not contradict the finding that the low affinity (monomeric) receptors dimerize upon EGF binding. In addition, the low affinity receptors can be recruited after activation of the high affinity subpopulation, if one assumes that the potential for intermolecular phosphorylation and for progressive oligomerization (mediated conceivably via cytoskeletal interactions) exists in the EGFR population as a whole. For example, the reduced translation (37) and rotational (59) mobilities of the high affinity EGFR are also evidenced in the total EGFR population after exposure to 37°C (37, 59, 61). Likewise, the requirement for full-length receptor aggregation proposed in a study of TKR activation by a host of nonspecific factors (35) can be reformulated in terms of reorientations restricted to the cytoplasmic domains of the EGFR. Conversely, the TKR activation (38) or dimerization inhibition (58) capacity of mAbs binding to the external domain at sites other than that occupied by EGF, as well as the potentiating effect of introducing a covalent interreceptor linkage in the extracellular domain (45), can be explained in terms of either stabilization or destabilization/inhibition of the active stereochemical structure as outlined in the scheme in Fig. 9.

In conclusion, we have shown the temperature-dependent EGF-induced microclustering of the EGFR and have

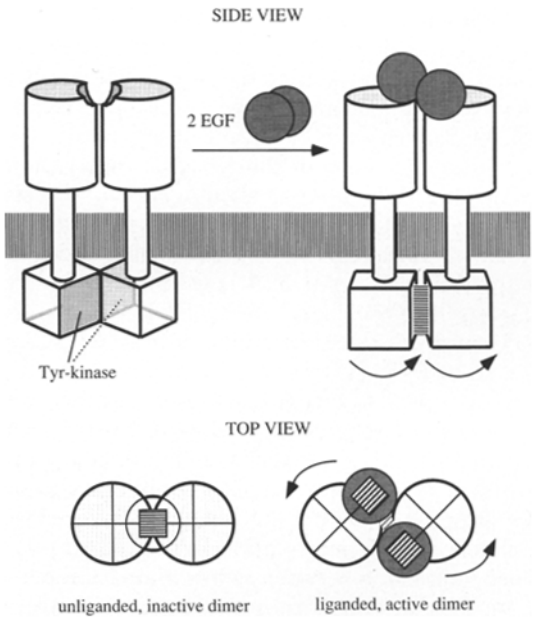


*Figure 9.* 'Twist' model for ligand-dependent activation of preformed EGFR dimers. Two unliganded monomers associate into a dimeric receptor with a preferential orientation. Ligand (*EGF*) binding leads to stereochemical exclusion and/or preferred orientation between the EGF ligands, requiring and accompanied by a mutual rotation (*twist*) of the two receptor monomers (*all domains*), and thereby leading to a corresponding reorientation and consequent activation of the tyrosine kinase. Conformational changes in the external domains and/or the ligands are not required, but one must assume a rigid relationship between the extracellular and cytoplasmic domains of the EGFR monomers. For further explanation, see Discussion.

provided evidence for a dimerized state of the high affinity EGFR subclass on A431 cells. The proposed stereochemical model provides an alternative for the allosteric activation model proposed by Ullrich and Schlessinger (40, 50) in the sense that the functional state of the EGFR is a preformed but inactive dimer in the absence of EGF. We note by way of comparison that the covalently dimerized insulin receptor (homologous to an EGF receptor dimer) can be activated after insulin binding (50). Hence, ligand-induced intersubunit interactions in the extracellular domain transduced via rigid structures to intracellular domains may be a general feature of the TKR family.

## *Appendix: Calculation of Minimal Receptor Dimerization from Photobleaching Curves*

Three assumptions are made: a two-state model: the receptor is present either as a monomer or as a dimer; neither the monomeric nor the dimeric receptor forms discriminate between donor and acceptor-labeled ligand (i.e., Fl-EGF and Rh-EGF); and an increase in photobleaching time only occurs when donor and acceptor-labeled ligands are present simultaneously on one receptor dimer.

The fraction of donor ligand involved in energy transfer ($f_{ET}$) is given by

$$f_{ET} = f_a \alpha, \tag{A1}$$

where $\alpha$ is the fraction of dimerized receptor and $f_a$ is the fraction of acceptor-labeled ligand. Suppose that in the absence of acceptor (no energy transfer) energy transfer the photobleaching time constant is $\tau_1$ and in the presence of acceptor potentiating energy transfer it is $\tau'_1$. Then the actual decay curve is given by

$$F(t) = f_{ET}\frac{\tau_1}{\tau'_1}\exp\left(-\frac{t}{\tau'_1}\right) + (1 - f_{ET})\exp\left(-\frac{t}{\tau_1}\right) \tag{A2}$$

In principle, $\tau_1$ and $\tau'_1$ can be very close, so that a double exponential fit will lead to errors. For this reason we fit our data to a single exponential decay function (see also 33) given by

$$F_{fit}(t) = a\exp\left(-\frac{t}{\tau_{eff}}\right). \tag{A3}$$

The discrepancy between F(t) and $F_{fit}(t)$ is minimized by defining and manipulating the difference function $V(a,\tau_{eff})$.

$$V(a, \tau_{eff}) = \int_{t=0}^{\infty} \{F(t) - F_{fit}(t)\}^2 dt \tag{A4}$$

V is minimized for $\frac{\partial V(a, \tau_{eff})}{\partial a} = \frac{\partial V(a, \tau_{eff})}{\partial \tau_{eff}} = 0.$

By solving the equations for both partial derivatives, $f_{ET}$ can be expressed as a function of $\tau_1$, $\tau'_1$ and $\tau_{eff}$.

$$f_{ET} = \left[\left(\frac{\tau_1 + \tau_{eff}}{\tau'_1 + \tau_{eff}}\right)^2\left(\frac{\tau'_1 - \tau_{eff}}{\tau_{eff} - \tau_1}\right) + 1\right]^{-1} \tag{A5}$$

In principle $\tau'_1$ cannot be determined experimentally since 100% of the receptors must be dimerized, and 100% of these dimerized receptors must be labeled with donor and acceptor ligand on either site. On the other hand, $\tau_1$ and $\tau_{eff}$ can be determined experimentally. Eq. A5 can be rewritten in terms of measured (E) and maximal ($E_{max}$) energy transfer by defining

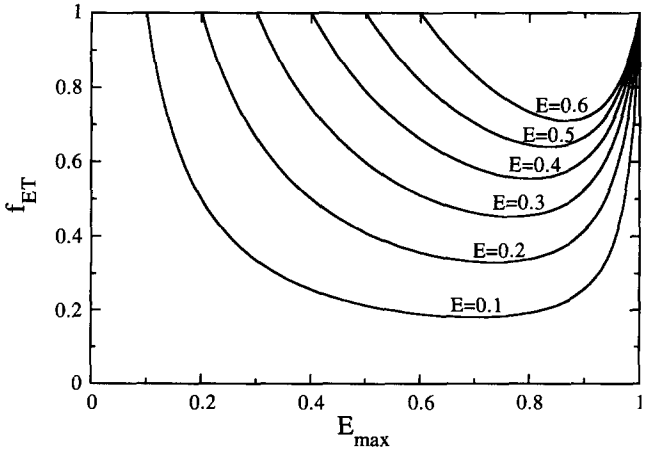


*Figure A 10.* Relationship between $f_{ET}$, E and $E_{max}$.

$$E = 1 - \frac{\tau_1}{\tau_{eff}} \tag{A6}$$

$$E_{max} = 1 - \frac{\tau_1}{\tau'_1}. \tag{A7}$$

Substitution of A6 and A7 into Eq. A5 leads to

$$f_{ET} = \left[\left(\frac{2 - E}{2 - E - E_{max}}\right)^2 \left(\frac{E_{max}}{E} - 1\right)(1 - E_{max}) + 1\right]^{-1}. \tag{A8}$$

In Fig. A10, $f_{ET}$ is plotted as a function of $E_{max}$ at several values of E. It is obvious that $f_{ET}$ goes through a minimum. This observation is interesting as one can state that at a given value of E (which can be determined experimentally), $f_{ET}$ must be greater or equal to this minimal value. This value is found by setting the partial derivative of $f_{ET}$ with respect to $E_{max}$ to zero and solving for $E_{max}$ (Eq. A9).

$$\frac{\partial f_{ET}}{\partial E_{max}} = 0 \Rightarrow (E_{max})_{\text{at minimum}} = \frac{2 + E}{3} \tag{A9}$$

By substitution of this $E_{max}$ value into Eq. A8, the minimal fraction $f_{ET}$ is obtained.

$$(f_{ET})_{minimum} = \frac{8E}{(E + 2)^2} \tag{A10}$$

Substitution of Eq. A1 into Eq. A10 leads to Eq. 2 in the text.

Received for publication 8 November 1994 and in revised form 22 February 1995.

### *References*


1. Azevedo, J. R., and D. A. Johnson. 1990. Temperature dependent lateral and transverse distribution of the epidermal growth factor receptors in A431 plasma membranes. *J. Membr. Biol.* 118:215–224.
2. Bellot, F. W., R. Moolenaar, B. Kris, I. Mirakhur, A. Verlaan, J. Ullrich, J. Schlessinger, and S. Felder. 1990. High-affinity epidermal growth factor binding is specifically reduced by a monclonal antibody and appears to be neccesary for early responses. *J. Cell Biol.* 110:491–502.
3. Böni-Schnetzler, M., and P. F. Pilch. 1987. Mechanism of epidermal growth factor receptor autophosphorylation and high-affinity binding. *Proc. Natl. Acad. Sci. USA.* 84:7832–7836.
4. Brown, M. S., and J. L. Goldstein. 1979. Receptor-mediated endocytosis: insights from the lipoprotein receptor system. *Proc. Natl. Acad. Sci. USA.* 76:3330–3337.
5. Carpenter, G. 1992. Receptor tyrosine kinase substrates: *src* homology domains and signal transduction. *FASEB (Fed. Am. Soc. Exp. Biol.) J.* 6: 3283–3289.
6. Carpenter, G. 1987. Receptors for epidermal growth factors and other polypeptide mitogens. *Annu. Rev. Biochem.* 56:881–914.
7. Carpenter, G., and S. Cohen. 1990. Epidermal growth factor. *J. Biol. Chem.* 265:7709–7712.
8. Carraway III, K. L., and R. A. Cerione. 1991. Comparison of epidermal growth factor (EGF) receptor-receptor interactions in intact A431 cells and isolated plasma membranes. *J. Biol. Chem.* 266:8899–8906.
9. Carraway III, K. L., and R. A. Cerione. 1993. Fluorescent-labeled growth factor molecules serve as probes for receptor binding and endocytosis. *Biochemistry.* 32:12039–12045.
10. Carraway III, K. L., and R. A. Cerione. 1993. Inhibition of epidermal growth factor receptor aggregation by an antibody directed against the epidermal growth factor receptor extracellular domain. *J. Biol. Chem.* 268:23860–23867.
11. Carraway III, K. L., J. G. Koland, and R. A. Cerione. 1989. Visualization of epidermal growth factor (EGF) receptor aggregation in plasma membranes by fluorescence resonance energy transfer. *J. Biol. Chem.* 264: 8699–8707.
12. Clegg, R. M., B. Fedderson, E. Gratton, and T. M. Jovin. 1992. Time resolved imaging fluorescence microscopy. *SPIE Proc.* 1604:448–460.
13. Cochet, C., O. Kashles, E. M. Chambaz, I. Borrello, C. R. King, and J. Schlessinger. 1988. Demonstration of epidermal growth factor-induced receptor dimerization in living cells using a chemical covalent cross-linking agent. *J. Biol. Chem.* 263:3290–3295.
14. Defize, L. H. K., D. J. Arndt-Jovin, T. M. Jovin, J. Boonstra, J. Meisenhelder, T. Hunter, H. T. de Hey, and S. W. de Laat. 1988. A431 cell variants lacking the blood group A antigen display increased high affinity epidermal growth factor receptor number, protein-tyrosin kinase activity, and receptor turnover. *J. Cell Biol.* 107:939–949.
15. Defize, L. H. K., J. Boonstra, J. Meisenhelder, W. Kruijer, L. G. J. Tertoolen, B. C. Tilly, T. Hunter, P. M. P. van Bergen en Henegouwen, W. H. Moolenaar, and S. W. de Laat. 1989. Signal transduction by epidermal growth factor occurs through the subclass of high affinity receptors. *J. Cell Biol.* 109:2495–2507.
16. Fabricant, R. N., J. E. De Larco, and G. J. Todaro. 1977. Nerve growth factor receptors on human melenoma cells. *Proc. Natl. Acad. Sci. USA.* 74: 565–569.
17. Fanger, B. O., K. S. Austin, H. S. Earp, and J. A. Cidlowski. 1986. Crosslinking of epidermal growth factor receptors in intact cells: detection of initial stages of receptor clustering and determination of molecular weight of high-affinity receptors. *Biochemistry.* 25:6414–6420.
18. Fanger, B. O., J. E. Stephens, and J. V. Staros. 1989. High yield trapping of EGF-induced receptor dimers by chemical cross-linking. *FASEB (Fed. Am. Soc. Exp. Biochem.) J.* 3:71–75.
19. Friedman, B., A. R. J. Frackelton, A. H. Ross, J. M. Connors, H. Fujiki, T. Sugiura, and M. R. Rosner. 1984. Tumor promotors block tyrosine-specific phosphorylation of the epidermal growth factor receptor. *Proc. Natl. Acad. Sci. USA.* 81:3034–3038.
20. Gadella, T. W. J., Jr., R. M. Clegg, and T. M. Jovin. 1994. Fluorescence lifetime imaging microscopy: pixel-by-pixel analysis of phase-modulation data. *Bioimaging.* 2:139–159.
21. Gadella, T. W. J., Jr., T. M. Jovin, and R. M. Clegg. 1993. Fluorescence lifetime imaging microscopy (FLIM): spatial resolution of microstructures on the nanosecond time scale. *Biophys. Chem.* 48:221–239.
22. Goldstein, J. L., R. W. G. Anderson, and M. S. Brown. 1979. Coated pits, coated vesicles, and receptor-mediated endocytosis. *Nature (Lond.).* 279: 679–685.
23. Greenfield, C., I. Hiles, M. D. Waterfield, M. Federwisch, A. Wollmer, T. L. Blundell, and N. McDonald. 1989. Epidermal growth factor binding induces a conformational change in the external domain of its receptor. *EMBO (Eur. Mol. Biol. Organ.) J.* 8:4115–4123.
24. Gronowski, A. M., and P. J. Bertics. 1993. Evidence for the potentiation of epidermal growth factor receptor tyrosine kinase activity by association with the detergent-insoluble cellular cytoskeleton: analysis of intact and carboxy-terminally truncated receptors. *Endocrinology.* 133:2838–2846.
25. Haigler, H. T., J. A. McKanna, and S. Cohen. 1979. Rapid stimulation of pinocytosis in human carcinoma cells A-431 by epidermal growth factor. *J. Cell Biol.* 81:382–395.
26. Hellen, E. H., and D. Axelrod. 1991. Kinetics of epidermal growth factor/receptor binding on cells measured by total internal reflection/fluorescence recovery after photobleaching. *J. Fluoresc.* 1:113–128.
27. Hillman, G. M., and J. Schlessinger. 1982. Lateral diffusion of epidermal growth factor receptor complexed to its surface receptor does not account for the thermal sensitivity of patch formation and endocytosis. *Biochemistry.* 21:2659–2663.
28. Jovin, T. M., and D. J. Arndt-Jovin. 1989. FRET microscopy: digital imaging of fluorescence resonance energy transfer. Application in cell biology. *In* Cell Structure and Function by Microspectrofluorometry. E. Kohen and J. G. Hirschbergs, editors. Academic Press Inc., San Diego, CA. pp. 99–117.
29. Jovin, T. M., and D. J. Arndt-Jovin. 1989. Luminescence digital imaging microscopy. *Annu. Rev. Biophys. Biophys. Chem.* 18:271–308.
30. Jovin, T. M., D. J. Arndt-Jovin, G. Marriot, R. M. Clegg, M. Robert-Nicoud, and T. Schormann. 1990. Distance, wavelength and time: the versatile 3rd dimensions in light emission microscopy. *In* Optical Microscopy for Biology. B. Herman and K. Jacobson, editors. Wiley-Liss, NY. pp. 575–602.
31. Kim, S. H. 1994. "Frozen" dynamic dimer model for transmembrane signaling in bacterial chemotaxis receptors. *Protein Sci.* 3:159–165.
32. Knighton, D. R., D. L. Cadena, J. Zheng, L. F. Ten-Eyck, S. S. Taylor, J. M. Sowadski, and G. N. Gill. 1993. Structural features that specify tyrosine kinase activity deduced from homology modeling of the epidermal growth factor receptor. *Proc. Natl. Acad. Sci. USA.* 90:5001–5005.
33. Kubitscheck, U., M. Kircheis, R. Schweitzer-Stenner, W. Dreybrodt, T. M. Jovin, and I. Pecht. 1991. Fluorescence resonance energy transfer on single living cells: application to binding of monovalent haptens to cell-bound immunoglobulin E. *Biophys. J.* 60:307–318.
34. Marx, J. 1993. Two major signal pathways linked. *Science (Wash. DC).* 262: 988–990.
35. Mohammadi, M., A. Honegger, A. Sorokin, A. Ullrich, J. Schlessinger, and D. R. Hurwitz. 1993. Aggregation-induced activation of the epidermal growth factor receptor protein tyrosine kinase. *Biochemistry.* 32:8742–8748.
36. Moodie, S. A., B. M. Willumsen, M. J. Weber, and A. Wolfman. 1993. Complexes of Ras. GTP with Raf-1 and mitogen-activated protein kinase kinase. *Science (Wash. DC).* 260:1658–1661.
37. Rees, A. R., M. Gregoriou, P. Johnson, and P. B. Garland. 1984. High affinity epidermal growth factor receptors on the surface of A431 cells have

restricted lateral diffusion. *EMBO (Eur. Mol. Biol. Organ.) J.* 3:1843–1847.
38. Reins, H. A., G. Steinhilber, B. Freiberg, and F. A. Anderer. 1993. Anti-epidermal growth factor receptor monoclonal antibodies affecting signal transduction. *J. Cell. Biochem.* 51:236–248.
39. Schlessinger, J. 1980. The mechanism and role of hormone-induced clustering of membrane receptors. *Trends Biochem. Sci.* 5:210–214.
40. Schlessinger, J. 1988. Signal transduction by allosteric receptor oligomerization. *TIBS.* 13:443–447.
41. Schlessinger, J. 1993. How receptor tyrosine kinases activate Ras. *TIBS.* 18: 273–275.
42. Schlessinger, J., Y. Shechter, M. C. Willingham, and I. Pastan. 1978. Direct visualization of binding, aggregation, and internalization of insulin and epidermal growth factor receptors on living fibroblastic cells. *Proc. Natl. Acad. Sci. USA.* 75:2659–2663.
43. Schlessinger, J., and A. Ullrich. 1992. Growth factor signaling by receptor tyrosine kinases. *Neuron.* 9:383–391.
44. Sierke, S. L., and J. G. Koland. 1993. SH2 domain proteins as high-affinity receptor tyrosine kinase substrates. *Biochemistry.* 32:10102–10108.
45. Sorokin, A., M. A. Lemmon, A. Ullrich, and J. Schlessinger. 1994. Stabilization of an active dimeric form of the epidermal growth factor receptor by introduction of an inter-receptor disulfide bond. *J. Biol. Chem.* 269: 9752–9759.
46. Spaargaren, M., L. H. K. Defize, J. Boonstra, and S. W. De Laat. 1991. Antibody-induced dimerization activates the epidermal growth factor tyrosin kinase. *J. Biol. Chem.* 266:1733–1739.
47. Staros, J. V. 1988. Membrane-impermeant cross-linking reagents: probes of the structure and dynamics of membrane proteins. *Accounts Chem. Res.* 21:435–441.
48. Stern, D. F., M. P. Kamps, and H. Lao. 1988. Oncogenic activation of p185neu stimulates tyrosin kinase phosphorylation *in vivo*. *Mol. Cell. Biol.* 8:3969–3973.
49. Ullrich, A., L. Coussemns, J. S. Hayflick, T. J. Dull, A. Gray, A. W. Tam, J. Lee, Y. Yarden, T. A. Libermann, J. Schlessinger, et al. 1984. Human epidermal growth factor receptor cDNA sequence and aberrant expression of the amplified gene in A431 epidermoid carcinoma cells. *Nature (Lond.).* 309:418–425.
50. Ullrich, A., and J. Schlessinger. 1990. Signal transduction by receptors with tyrosine kinase activity. *Cell.* 16:203–212.
51. van Belzen, B., P. J. Rijken, W. J. Hage, S. W. De Laat, A. J. Verkleij, and J. Boonstra. 1988. Direct visualization and quantitative analysis of epidermal growth factor-induced clustering. *J. Cell. Physiol.* 134:413–420.
52. van Bergen en Henegouwen, P. M. P., L. H. K. Defize, J. de Kroon, H. van Damme, A. J. Verkleij, and J. Boonstra. 1989. Ligand-induced association of epidermal growth factor receptor to the cytoskeleton of A431 cells. *J. Cell. Biochem.* 39:455–465.
53. Wiegant, F. A. C., F. J. Blok, L. H. K. Defize, W. A. M. Linnemans, A. J. Verkley, and J. Boonstra. 1986. Epidermal growth factor receptors associated to cytoskeletal elements of epidermoid carcinoma (A431) cells. *J. Cell Biol.* 103:87–94.
54. Willingham, M. C., H. T. Haigler, D. J. Fitzgerald, M. G. Gallo, A. V. Rutherford, and I. H. Pastan. 1983. The morphologic pathway of binding and internalization of epidermal growth factor in cultured cells. Studies in A431, KB and 3T3 cells using multiple methods of labeling. *Exp. Cell Res.* 146:163–175.
55. Wofsy, C., B. Goldstein, K. Lund, and H. S. Wiley. 1992. Implications of epidermal growth factor (EGF) induced EGF receptor aggregation. *Biophys. J.* 63:98–110.
56. Yarden, Y., and J. Schlessinger. 1987. Epidermal growth factor receptor induces rapid, reversible aggregation of the purified epidermal growth factor receptor. *Biochemistry.* 26:1443–1451.
57. Yarden, Y., and J. Schlessinger. 1987. Self-phosphorylation of the epidermal growth factor receptor: evidence for a model of intramolecular allosteric activation. *Biochemistry.* 26:1434–1442.
58. Zhou, M., S. Felder, M. Rubinstein, D. R. Hurwitz, A. Ullrich, I. Lax, and J. Schlessinger. 1993. Real-time measurements of kinetics of EGF binding to soluble EGF receptor monomers and dimers support the dimerization model for receptor activation. *Biochemistry.* 32:8193–8198.
59. Zidovetzki, R., D. A. Johnson, D. J. Arndt-Jovin, and T. M. Jovin. 1991. Rotational mobility of high-affinity epidermal growth factor receptors on the surface of living A431 cells. *Biochemistry.* 30:6162–6166.
60. Zidovetzki, R., Y. Yarden, J. Schlessinger, and T. M. Jovin. 1986. Microaggregation of hormone-occupied epidermal growth factor receptors on plasma-membrane preparations. *EMBO (Eur. Mol. Biol. Organ.) J.* 5: 247–250.
61. Zidovetzki, R., Y. Yarden, J. Schlessinger, and T. M. Jovin. 1981. Rotational diffusion of epidermal growth factor receptor complexed to cell surface receptors reflects rapid microaggregation and endocytosis of occupied receptors. *Proc. Natl. Acad. Sci. USA.* 79:6981–6985.